Research Paper

A Fluorescence-Guided Laser Ablation System for Removal of Residual Cancer in a Mouse Model of Soft Tissue Sarcoma

Alexander L. Lazarides[1*], Melodi J. Whitley[1,2*], David B. Strasfeld[3], Diana M. Cardona[4], Jorge M. Ferrer[3], Jenna L. Mueller[5], Henry L. Fu[5], Suzanne Bartholf DeWitt[6], Brian E. Brigman[6], Nimmi Ramanujam[5], David G. Kirsch[2,7], William C. Eward[6✉]

1. School of Medicine, Duke University, Durham, North Carolina
2. Department of Pharmacology & Cancer Biology, Duke University Medical Center, Durham, North Carolina
3. Lumicell, Inc., Wellesley, MA
4. Department of Pathology, Duke University Medical Center, Durham, North Carolina
5. Department of Biomedical Engineering, Duke University, Durham, North Carolina
6. Department of Orthopaedic Surgery, Duke University Medical Center, Durham, North Carolina
7. Department of Radiation Oncology, Duke University Medical Center, Durham, North Carolina

* Co-first authors

✉ Corresponding author: William C Eward MD, DVM, Department of Orthopaedic Surgery, Duke University Medical Center, Box 3312 DUMC, Durham, NC 27710, Phone: 919.681.6982; Fax: 919.681.7645; E-mail: william.eward@dm.duke.edu.

Abstract

The treatment of soft tissue sarcoma (STS) generally involves tumor excision with a wide margin. Although advances in fluorescence imaging make real-time detection of cancer possible, removal is limited by the precision of the human eye and hand. Here, we describe a novel pulsed Nd:YAG laser ablation system that, when used in conjunction with a previously described molecular imaging system, can identify and ablate cancer *in vivo*. Mice with primary STS were injected with the protease-activatable probe LUM015 to label tumors. Resected tissues from the mice were then imaged and treated with the laser using the paired fluorescence-imaging/ laser ablation device, generating ablation clefts with sub-millimeter precision and minimal underlying tissue damage. Laser ablation was guided by fluorescence to target tumor tissues, avoiding normal structures. The selective ablation of tumor implants *in vivo* improved recurrence-free survival after tumor resection in a cohort of 14 mice compared to 12 mice that received no ablative therapy. This prototype system has the potential to be modified so that it can be used during surgery to improve recurrence-free survival in patients with cancer.

Key words: Fluorescence Imaging, Laser Ablation, Sarcoma, Local Neoplasm Recurrence, Image-Guided Surgery

Introduction

During resection of a soft tissue sarcoma (STS), the surgeon attempts to remove the tumor with a margin of normal tissue in order to increase the likelihood that no malignant cells remain. In doing so, the surgeon must balance the risk of resecting too much tissue, thereby impairing function, or resecting too little tissue and leaving the patient at risk for recurrence of disease. Currently, frozen section analysis allows for intraoperative margin assessment, but this technique is subject to sampling bias and error [1]. Complete histopathological assessment of margins is made in the days to weeks following surgery. In the setting of a positive margin, additional treatment such as re-operation or adjuvant radiation therapy must be

undertaken, which carry the risk of increased morbidity. Even in the case of a negative final surgical margin, STS of the extremity treated with limb-sparing surgery alone still recur locally in at least 25% of patients [2]. We have previously shown the efficacy of using protease-activated tumor-selective fluorescent probes to label and intraoperatively detect microscopic residual disease within the tumor bed in preclinical models of STS surgery [3, 4]. A phase I clinical trial of one protease-activated probe, LUM015 (Lumicell, MA), has recently been completed (NCT01626066), showing that LUM015 is safe in humans and results in tumor-specific fluorescence [5]. While LUM015 preferentially labels sarcoma over normal tissue in mice, dogs and humans, removing any residual cancer identified by the device is restricted by the precision limits of the surgeon's eyes and hands [6].

Several types of fluorescent imaging agents have been developed that target tumors via various mechanisms including receptor/antigen affinity and tumor-specific enzyme activity, such as proteases and telomerase [7]. Some of these imaging agents can serve a dual purpose, by not only acting as a tumor marker, but also allowing tumor-specific killing of cells. For example, photodynamic therapy (PDT) couples light exposure with tumor-targeted photosensitizing fluorophores to induce apoptosis in tumor cells [8, 9]. On the other hand, tumor-labeling agents can be inherently lethal. Yano et al showed that selective targeting of tumor cells using a telomerase-dependent adenovirus expressing green fluorescence protein can not only aid the surgeon in detecting tumor cells but may result in the killing of residual cancer in an orthotopic mouse model of sarcoma [10]. In this study, we show the coupling of a protease-activated tumor-specific fluorescent probe, LUM015, with fluorescence-targeted laser ablation to identify and destroy residual tumor cells within the tumor bed.

Intraoperative laser ablation has been utilized previously in surgical oncology, but such approaches are guided by the surgeon's visual recognition of structures, and therefore restricted to macroscopic objects [11, 12]. Fluorescence imaging with a cancer specific imaging agent, coupled with a highly sensitive charge coupled device (CCD), permits the detection of microscopic disease [3]. Here, we developed a prototype system that couples pulsed Nd:YAG laser ablation with a fluorescence imaging system to guide the laser beam to selectively target areas of high fluorescence corresponding to residual disease.

The purpose of this study was to provide proof of principle for a combined fluorescence imaging and laser ablation device to decrease rates of local recurrence. To test the device, we used primary sarcomas that developed in genetically engineered mice with conditional expression of oncogenic *K-ras* or *B*-raf and deletion of *p53* [13]. In this temporally and spatially restricted model, the location of the sarcoma is limited within the extremity to facilitate experiments to image and treat the tumor. First, we injected sarcoma-bearing mice with LUM015 and resected sarcoma tissue in order to characterize the fluorescence-guided ablation system. We then performed *in vivo* fluorescence guided ablation on tumor implants in this same mouse model to observe its impact on recurrence free survival.

Materials and Methods

Mice and Sarcoma Generation

Mouse work was performed in accordance with the Duke University Institutional Animal Care and Use Committee approved protocols. Primary STS were generated using the previously described alleles, $p53^{Fl}$ [14], $Braf^{Ca}$ [15], and $LSL\text{-}Kras^{G12D}$ [16]. Tumors were initiated by intramuscular injection of adenovirus expressing Cre-recombinase as previously described [17] into the hind limb of mice with the genotype $Braf^{Ca/+}$; $p53^{Flox/Flox}$ or $LSL\text{-}YFP$; $LSL\text{-}Kras^{G12D/+}$, $p53^{Flox/Flox}$. Surgery was performed when tumors reached approximately 1 cm^3 in size.

The Laser Ablation System

Tissue ablation was achieved using a pulsed, 1064 nm Nd:YAG laser (CryLas, Germany). This laser selected for ease of incorporation into the fluorescence imaging system and previous data showing ablation of neural tissue [18], porcine skin [19] and myocardium [20] with minimal thermal damage to surrounding tissue. The laser was focused to a 500-μm diameter spot, yielding a photon flux of 0.36 GW/cm^2 that was adequate for achieving plasma-mediated ablation [20, 21], allowing for minimized thermal necrosis and high dimensional precision. Plasma mediation was confirmed by acoustic transients correlated with laser pulsing typical of plasma mediated tissue ablation and spectral characterization of the ablation plume. Secondary plasma radiation was characterized by collecting emission from the ablation plume using a fiber-coupled high-resolution spectrometer (HR2000, Ocean Optics, Florida).

We diagram the layout of the integrated system in **Figure 1A, B**. Briefly, excitation of LUM015 is achieved using flood illumination by a Xe lamp (SolarMaxx 300, Sunoptics, California) filtered to excite in the Cy5 absorption band (620±30 nm, Chroma, Vermont). Fluorescence emission from the Cy5 dye is collected by an f = 40 mm achromatic doublet (Thorlabs, New Jersey) and a 700±37.5 nm bandpass

emission filter (Chroma, Vermont), respectively, before being imaged at a 2048 x 2048 pixel CCD camera (RM4200 GE, JAI, California) by a 35 mm machine vision lens (Tamron, New York).

Direction of laser pulses onto the exact spot of detected fluorescence is accomplished as follows: (1) the ablation laser is introduced into the system collinearly with the axis of the imaging optics using a dichroic beamsplitter (Chroma, Vermont) that reflects 1064 nm light and transmits Cy5 fluorescence in the far red spectrum, (2) a pair of galvo-mirrors (Thorlabs, New Jersey) control the pointing direction of the ablation laser to determine the location of the laser focus within the specimen plane, (3) a translation stage permits vertical adjustment of the tissue plane over 25 mm with 25 μm precision to control the ablation depth. The entire assembly of the prototype system is housed in a photo-protective box (not shown).

The CCD, galvo-mirrors and pulsed Nd:YAG laser were all connected and controlled by a custom software program coded in the LabVIEW Development System (National Instruments, Texas). This program interfaced with a data acquisition board from National Instruments to send analog signals to the galvo-mirrors and a digital signal to the pulsed Nd:YAG laser to control laser pointing direction and pulsing, respectively. The CCD interfaced with the computer using standard GigE vision framework. The entire process occurs in real time.

Measuring fluorescence at different depths

In order to simulate thick *in vivo* tissue, a set of tissue phantoms were constructed by homogeneous mixing of titanium dioxide (TiO_2, Sigma-Aldrich, Missouri) and polydimethylsiloxane (PDMS, Dow Corning, Michigan) as described previously [22]. Briefly, tissue phantoms were create by mixing 2.25 grams of TiO_2 per gram of PDMS [23]. This resulted in phantoms with a reduced scattering coefficient (μ'_s) of 10 cm^{-1}, which is the μ'_s of most soft tissues [24, 25]. The phantoms were constructed in a petri dish with a cover glass window on the bottom (Mattek, Massachusetts) by filling the dish with 0, 2, 4, 6, 8, or 10 mm of the PDMS/TiO_2 mixture. Each phantom was placed in a vacuum chamber in order to remove residual air bubbles created during mixing. To measure fluorescence at different depths, two pieces of tumor were harvested from a mouse with primary STS six hours after administration of 3.5 mg/kg LUM015 via tail vein. These pieces were placed under the cover glass window of each phantom petri dish and fluorescence was measured using the LUM imaging device. The background fluorescence of the 10 mm phantom was also determined as a baseline measurement.

Quantifying the Effect of Laser Ablation on Tissue

3.5 mg/ kg of LUM015 was injected into the tail vein of 3 mice with primary STS. 3 tumor cubes were obtained from each mouse tumor (9 cubes total) 6 hours following injection. Each set of tumor cubes was then imaged with the laser ablation system and subjected to 1, 2 or 3 passes of the laser per cube. Tissue was then formalin-fixed and paraffin embedded (FFPE), sectioned perpendicularly to the ablated surface, and subject to hematoxylin and eosin staining (H&E). The sections were examined microscopically and the depth of ablation was determined.

Fluorescence-Guided Laser Ablation of Positive Tumor Margin Sections

Mice with primary STS were administered 3.5 mg/kg of LUM015 via tail vein. Tumor and tissue from the tumor margin were harvested 6 hours following injection, frozen in OCT, and sectioned. For every 150 μm thick section, we obtained an adjacent 10 μm section for histopathology. The tumor section was imaged with the integrated system to set a positive fluorescence threshold (80% of the minimum tumor fluorescence signal) [3]. We then used the integrated system to identify and ablate tissue on the tumor margin section with positive fluorescence. Finally, histopathological analysis of treated tissue sections was performed.

Harlaar et al. (2010) suggested that yellow fluorescent protein (YFP) fluorescence is the gold standard by which optical imaging and optical therapeutics should be evaluated [26]. Therefore, we crossed *LSL-Kras*$^{G12D/+}$, *p53*$^{Flox/Flox}$ mice with *LSL-YFP* mice to generate YFP-expressing sarcomas. These mice were administered LUM015 and tissues were harvested and sectioned as described above. Thick sections were imaged prior to ablation using a Leica DFX340 FX fluorescence microscope to measure Cy5 and YFP signals. Tumor margin sections were subject to the laser ablation system as described above and reevaluated post-treatment using fluorescence microscopy to correlate loss of Cy5 signal with loss of YFP signal.

Local Recurrence Studies

Mice with primary STS were administered 1.5 or 3.5 mg/kg of LUM015 via tail vein. Six hours after injection, mice were placed under anesthesia and a gross total tumor resection with negative margins was performed. The resected tumor and resulting tumor bed were imaged to establish the fluorescence threshold and confirm negative residual fluorescence in the tumor bed, respectively. In one cohort, no further procedures were done and the surgical wound was closed (- Implant/ - Laser Ablation, Figure 5A). In a

second cohort, a 3 mm^3 piece of the excised tumor was implanted in the tumor bed of the same mouse to simulate residual disease, the tumor bed was imaged, and the surgical wound was closed (+ Implant/ - Laser Ablation). In the third cohort, simulated residual disease was implanted as above followed by fluorescence-guided laser ablation of any fluorescence in the tumor bed above threshold and closure of the surgical wound (+ Implant/ + Laser Ablation). Tumor implants were confirmed by histopathology. All mice were monitored for local recurrence during the 100 days following surgery by twice-weekly inspection and palpation of the operative limb. Date of recurrence was noted when the tumor reached 1.5-2 cm in size. All suspected recurrences were confirmed by histopathological analysis of the tissue.

Reproduction of Intraoperative Images for Publication Display

For publication purposes, we adjusted the brightness and contrast of images so that readers could better appreciate differences in fluorescence signals. Brightness and contrast for all images from the same animal were adjusted in ImageJ based on the minimum and maximum pixel values of the tumor image.

Statistical Methodology

Results are presented as means +/- standard error of the mean (SEM) unless otherwise indicated. One-way ANOVA was used when measuring the effect of only one variable, such as number of laser passes. For the local recurrence study, Kaplan-Meir analysis was performed with the log-rank test for statistical significance. Significance was assumed at $P < 0.05$. All calculations were performed using Prism 6 (GraphPad).

Results

Imaging Device Design and Characterization

The pre-clinical laser ablation module is combined with an imaging system capable of detecting microscopic residual cancer. This technology was modified from a previously tested system [3], with imaging specifications to meet the demands of this laser ablation study. The lens combination yields a system magnification of 0.81x (**Figure 1A**) and the image is cropped to a 5.5 x 5.5 mm region in the center of the object plane (600 x 600 pixel region of the CCD) over which consistent ablation parameters are achieved. This field of view was well suited for examining the full tumor bed during surgery and identifying small, residual cancer features.

To characterize the resolution of this imaging system, an image of a 1951 USAF resolution target (Thorlabs, New Jersey) was taken at the center of the field of view (**Figure 1C**). Horizontal and vertical line spread functions were generated by differentiation over slices through a slanted edge, respectively. Horizontal and vertical modulation transfer functions (MTF) were subsequently generated by Fourier Transform into the frequency domain, yielding units of line pair/mm (lp/mm). The MTF was fit using a single exponential, which assumes a Lorentzian point spread function, yielding coefficients of determination of $r^2 = 0.994$ horizontally and $r^2 = 0.990$ vertically, supporting the validity of this model (**Figure 1D**). The Rayleigh criterion was used to determine the horizontal resolution, 54 lp/mm, and the vertical resolution, 47 lp/mm, as described previously [3]. Hence, the system can resolve 10 µm features of adequate brightness. We further determined that the response to fluorescence of the CCD was linear with regard to exposure time (**Figure 1E**).

Spectral characterization of the ablation plume was consistent with plasma mediated ablation. A spectrum of the secondary radiation emitted by the ablation plume from 400 to 800 nm, along with spectra of the excitation and emission filters, is provided in **Figure 1F**. A sharp peak in ablation plume spectrum at 656 nm corresponds to electronic transitions of neutral hydrogen and has been observed in other tissue ablation experiments [19]. The photons emitted by the ablation plume in the emission channel (662.5 – 737.5 nm) were used to calibrate the position of the ablation laser in the field of view.

Characterizing Depth of Fluorescence Detection and Laser Effect

To determine the effect of overlying tissue thickness on the ability to detect fluorescence from residual fluorescence that is deep to the surface, we used tissue phantoms with a reduced scattering coefficient (μ'_s) of 10 cm^{-1}, which is consistent with the scattering coefficient measured in most soft tissues [24, 25]. Tumor tissue was harvested from a mouse with primary STS six hours after administration of LUM015 and placed under tissue phantoms with varying thicknesses of 0, 2, 4, 6, 8, and 10 mm. The fluorescence of the tumor tissue was measured through the overlying phantom and the background fluorescence of the 10 mm phantom was also determined as a baseline measurement (**Figure 2A**). We found that fluorescence above background levels could be detected even underneath the 10 mm phantom and that tumor fluorescence was at least twice that of background fluorescence at a depth of 8 mm.
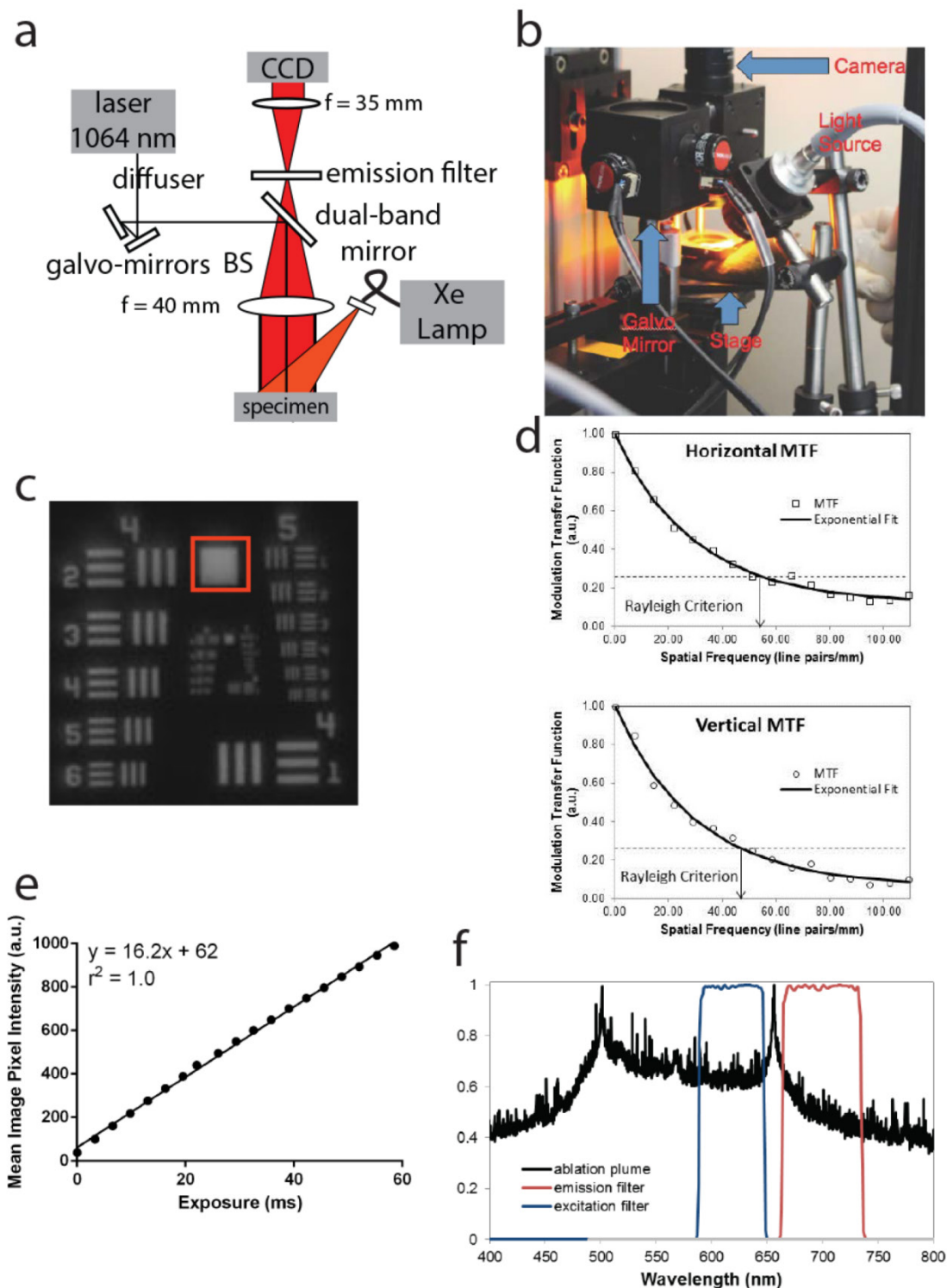
Figure 1. Paired imaging/laser ablation prototype and system characterization. These images illustrate and characterize the prototype system. (a) Optical layout of the integrated image detection and laser ablation system is shown. We use plasma-mediated ablation with a pulsed Nd:YAG laser, centered at 1064 nm for our design. A 1064 nm laser source is directed through a diffuser towards a series of motorized galvo-mirrors. These galvo-mirrors control the directionality of the laser output beam towards a dichroic mirror, which is subsequently directed towards a stage. A fiber bundle is connected to a xenon light source and attaches to the system to illuminate the specimen. Fluorescence emission from the sample is transmitted through the dichroic mirror and is spectrally filtered by a band-pass emission filter. An imaging lens focuses the fluorescence emission into a charge-coupled device (CCD). (b) Photograph of integrated image detection and laser ablation system. (c) Image of a standard US Air Force 1951 resolution target that was acquired by the prototype to determine the spatial resolution of the system. The region in the red box was used to generate the modulation transfer functions (MTF). (d) Horizontal and vertical modulation transfer functions are illustrated for the imaging system. The horizontal and vertical spatial frequency resolution limits are 54 lp/mm and 47 lp/mm, respectively. These correspond to approximately 10 μm of spatial resolution in both axes. (e) Pixel intensities acquired from a fluorescent standard imaged at different exposure times demonstrate a linear response of the device to exposure time (r^2=1.0, y=16.2x + 62). (f) A spectrum of the secondary radiation emitted by the ablation plume from 400 to 800 nm, along with spectra of the excitation and emission filters. A sharp peak at 656 nm in the ablation plume spectrum corresponds to electronic transitions of neutral hydrogen and has been observed in other tissue ablation experiments.
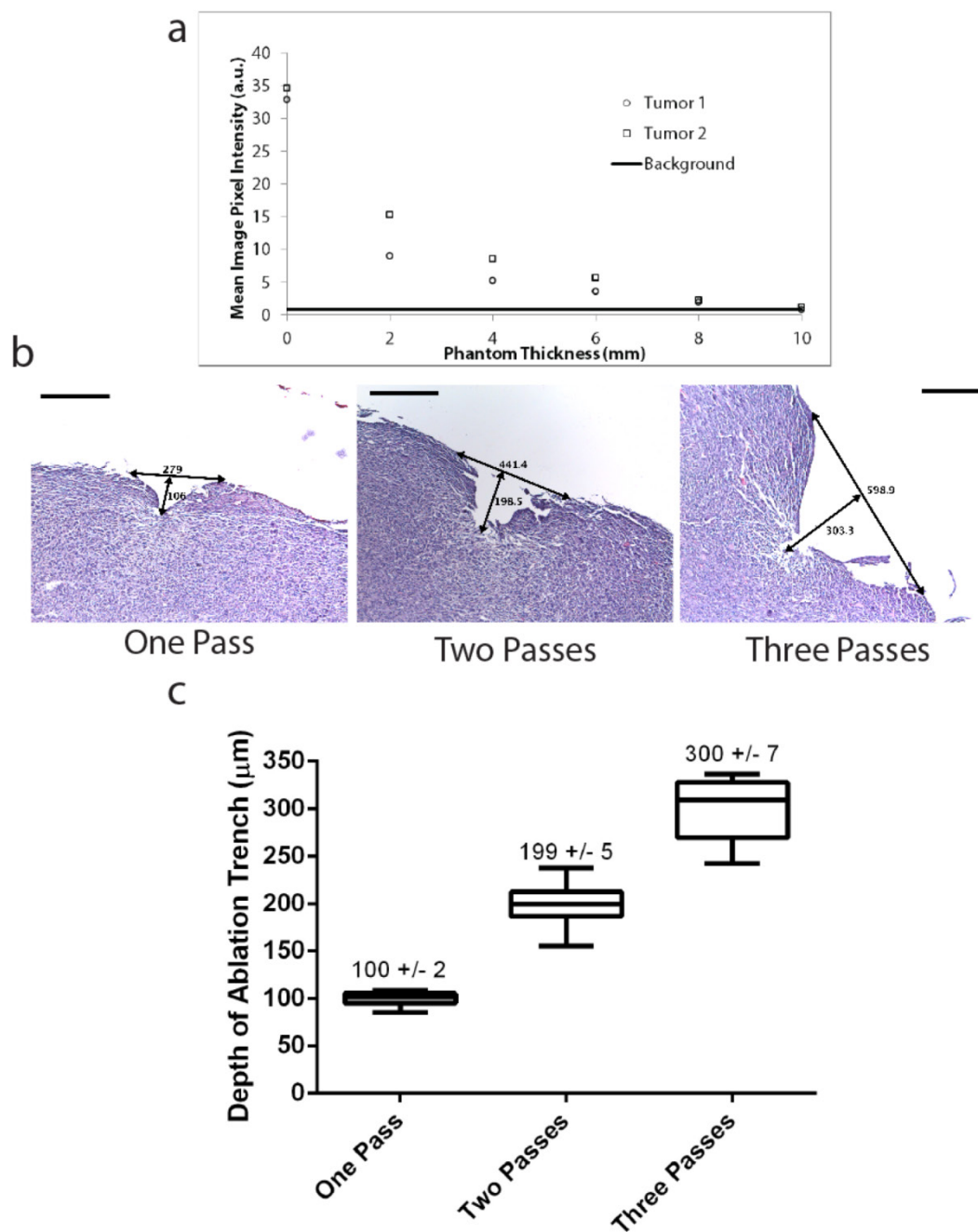
Figure 2. Deep tumor detection and laser ablation with sub-millimeter precision. (A) Two pieces of tumor tissue were harvested from a mouse with primary STS six hours injection of LUM015. These tumor pieces were placed under tissue phantoms of different thicknesses and the fluorescence was measured through the phantom. Background fluorescence of the 10 mm phantom was also determined as a baseline measurement. (B, C) Three mice with primary sarcomas were injected with LUM015 6 hours prior to harvesting tumor tissues. Three tumor cubes were taken from each mouse (9 cubes total), visualized with the laser ablation system and subjected to one, two or three passes of the laser. Each ablated tumor cube was then formalin fixed and paraffin embedded (FFPE) and cut into 10 μm sections. (B) Representative hematoxylin and eosin (H&E) stained sections of resected tumor pieces from mice showing the ablation trench that resulted from one, two and three passes of the ablation laser. The trench is identified with arrows indicating its dimensions in μm (Scale bar = 200). (C) A box plot of the ablation trench depth as a function of laser passes as measured on separate H&E sections, showing that the depth of ablation can be controlled with micron-level precision, depending on the number of passes (One-way ANOVA, $P<0.0001$).

In order to characterize laser depth precision and possible damage to adjacent tissue, we microscopically evaluated ablated tumor tissue. Three mice with primary STS were administered 3.5 mg/kg of LUM015 and sacrificed 6 hours after injection. Three tumor pieces were manually harvested from each mouse (9 pieces total) and then exposed to either one, two or three passes of the pulsed laser. Tumor pieces were then sectioned and stained with hematoxylin and eosin for histopathological evaluation to characterize the width and depth of the ablation cleft. Ablation of cancer cells via direct vaporization was visualized in the form of ablation clefts with minimal underlying thermal necrosis even after multiple passes of the laser (**Figure 2B**). A single pass of the laser resulted in an ablation cleft with a width of 290 +/- 11

μm and depth of 100 +/- 1.7 μm) (**Figure 2C**). Three ablation passes led to a mean ablation cleft that was 550 +/- 13 μm in width and 300 +/-7 μm in depth **(Figure 2C)**. These results show that the laser can be used to generate ablation trenches in a predictable and controlled manner with minimal damage to surrounding tissue.

Fluorescence Guided Laser Ablation of Cancer

Next, we tested whether the combined system could be utilized to ablate residual fluorescence with minimal collateral disruption of adjacent tissue. We injected 4 STS-bearing mice with 3.5 mg/kg LUM015 and sacrificed them 6 hours later. Tumor and tumor margin tissue was frozen and mounted onto slides (n=12). The integrated system was used to establish a pre-specified threshold by obtaining a fluorescence image of the tumor section (**Figure 3A**) and then identify and ablate areas of fluorescence above this threshold in the corresponding tumor margin section (**Figure 3B**). Fluorescence signal decreased in a manner that correlated with progressively larger areas of ablation (**Figure 3C, D**). This correlated well with histopathology, which revealed specific ablation of tumor tissue while preserving normal adjacent muscle (**Figure 3C, D**).
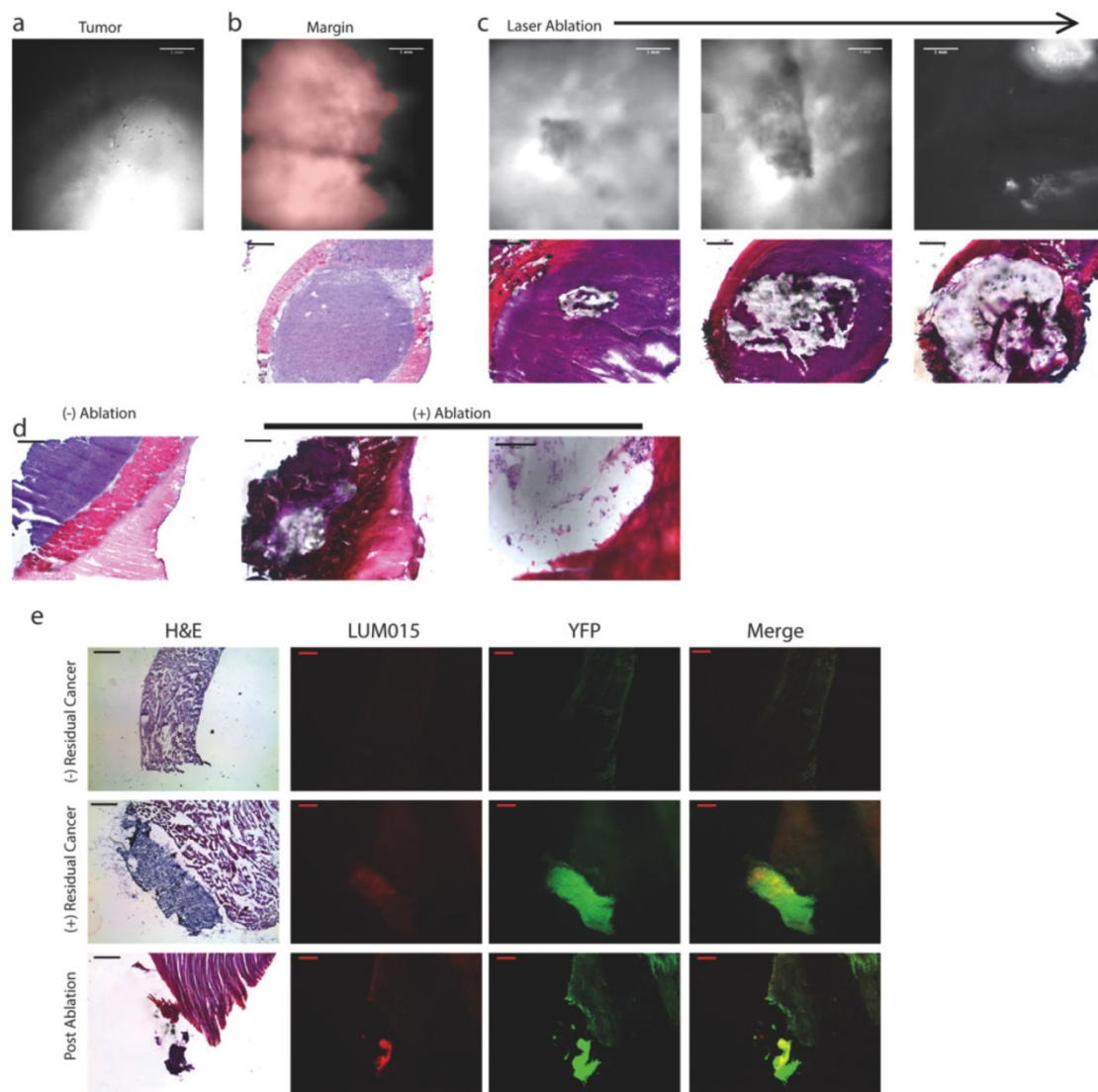
Figure 3. Tumor-selective tissue ablation with the paired fluorescence imaging/laser ablation device. In order to determine the ability to detect and ablate residual cancer, tumor margin sections from sarcoma-bearing mice injected with LUM015 were subject to image-guided laser ablation (n=12). Representative images are shown. **(a)** A 150 μm section of tumor tissue was imaged using the prototype device to establish a threshold for positive residual disease. **(b)** Then, a 150 μm section of the margin tissue was imaged to show areas of residual fluorescence that exceeded the threshold (highlighted in red). A corresponding 10 μm section was then subject to H&E staining to show a central area of tumor surrounded by normal tissues. **(c)** Serial 150 μm sections of margin tissue were then subject to increasing areas of fluorescence-guided laser ablation and subsequently H&E stained to show ablation of tumor tissue with preservation of surrounding normal muscle. **(d)** Another example of serial 150 μm margin sections with and without fluorescence-guided laser ablation. **(e)** Mice bearing YFP-expressing sarcomas were also used for fluorescence-guided laser ablation. These mice were injected with LUM015 followed by resection of the tumor and isolation of the resection margin. A sample of the resection margin was frozen and cut into 150 μm sections that were subject to fluorescence microscopy and fluorescence-guided laser ablation, followed by H&E staining and histological analysis. Margin sections without any residual disease showed low LUM015 and YFP signal (n=2). In margin sections that contained residual cancer, signal from LUM015 co-localized with signal from YFP-positive tumor cells (n=4). Partial laser ablation of these LUM015-positive areas resulted in focal loss of YFP signal and destruction of tumor tissue as observed on H&E. Scale bars = 500 μm unless otherwise noted.

To further determine the capacity of this system to specifically detect and ablate tumor tissue, we used a mouse sarcoma model that expresses yellow fluorescent protein (YFP) in the tumor cells (n=2 tumor-bearing mice). The mice were sacrificed 6 hours after administration of 3.5 mg/kg LUM015. Tumor and tumor margin samples were frozen and mounted onto slides (n=6). Prior to laser ablation, fluorescence microscopy of tissue sections showed co-localization of YFP and LUM015 signals. Using the combined imaging and laser ablation device, tumor tissue sec-

tions established the fluorescence threshold and tumor margin sections were treated with the laser if positive fluorescence was detected. Two tissue sections that demonstrated neither Cy5 nor YFP signal were shown to be muscle without tumor on histopathology (**Figure 3E**). Areas that had high levels of YFP expression were confirmed to be tumor tissue on histopathology (**Figure 3E**) in four slides. There was co-localization of YFP and Cy5 fluorescent regions. After laser ablation, Cy5 and YFP signals decreased (**Figure 3E**). Taken together, these results suggest that the integrated system can ablate areas of tumor identified with the imaging agent.

To investigate the potential to spare critical neurovascular structures adjacent to tumor, a mouse with a primary sarcoma surrounding the nerve was selected for laser ablation six hours after administration of 3.5 mg/kg LUM015. The resected tumor margin was frozen, sectioned and mounted onto slides (n=4 sections). As described above, the imaging system was used to guide laser ablation of tissue exhibiting fluorescence above the threshold established by imaging a section of the tumor (**Figure 4A**). This tissue was then subject to histopathological analysis. We identified areas on the margin sections that fell below the fluorescence threshold (**Figure 4B**) and corresponded to the presence of nerve within the tissue (**Figure 4C**). Because the laser was only activated for tissue that fell above the threshold, the nerve was spared from laser ablation (**Figure 4D**). This suggests that the system has the potential to be used to ablate residual sarcoma on or adjacent to critical neurovascular structures.

Figure 4. Intraoperative fluorescence-guided laser ablation may be used adjacent to critical neurovascular structures. In four 150 micron frozen margin sections, we observed areas of low fluorescence that corresponded with the presence of nerve (N) surrounded by areas of high fluorescence that corresponded to tumor (T). **(a)** Fluorescence image of the tumor obtained with the prototype system used for establishing the fluorescence threshold. **(b)** Fluorescence image of a margin section showing a region of fluorescence below the threshold. **(c)** H&E analysis of this section shows that the region of low fluorescence corresponds with the presence of a nerve (above: high magnification, below: low magnification). **(d)** Fluorescence-guided laser ablation allowed selective ablation of tumor tissue while sparing nerve tissue (above: high magnification, below: low magnification). H&E Scale bars = 500 μm for low magnification and 100 μm for high magnification.

Fluorescence Guided Laser Ablation Prevents Local Recurrence

We designed a proof-of-principle experiment to test the capacity of the integrated system to detect small volume disease in vivo and successfully ablate it (**Figure 5A**). Six hours prior to surgery, 46

mice with primary sarcomas were injected with LUM015 at a dose of 3.5 mg/kg. All mice received an amputation of the hind leg to obtain a wide negative margin and the tumor bed was imaged using the imaging device, which showed no residual fluorescence in the tumor bed in all 46 mice (**Figure 5B+C**). Five mice died in the early postoperative period. A cohort of 15 mice received no further treatment beyond the amputation (-Implant/ - Laser Ablation, **Figure 5C**). The wound was closed and the mice were followed for local recurrence for 100 days. In the remaining cohort of 26 mice, we simulated a positive margin by harvesting a 3 mm^3 autologous piece of known sarcoma from the resected tumor and implanted the tumor fragment back into the tumor bed of the same mouse. In all cases, implants were confirmed to be tumor by histopathological evaluation of a portion of the transplanted tissue. This cohort was subsequently randomized to receive either no further treatment (n=12, + Implant/ - Laser Ablation, **Figure 5D**) or in vivo laser ablation of fluorescence detected in the tumor bed containing the tumor implant (n=14, + Implant/ + Laser Ablation, **Figure 5E**). In the + Implant/ + Laser Ablation cohort, fluorescence in the tumor bed from the tumor implant was identified by a second operator using the imaging system. All fluorescence above the pre-specified threshold (80% of tumor minimum) was ablated in vivo with the laser until there was no longer residual fluorescence. In all three cohorts, the surgical wound was closed and the mice were followed for local recurrence. Kaplan-Meir analysis was performed to compare the three cohorts and the log-rank test was used for statistical significance.
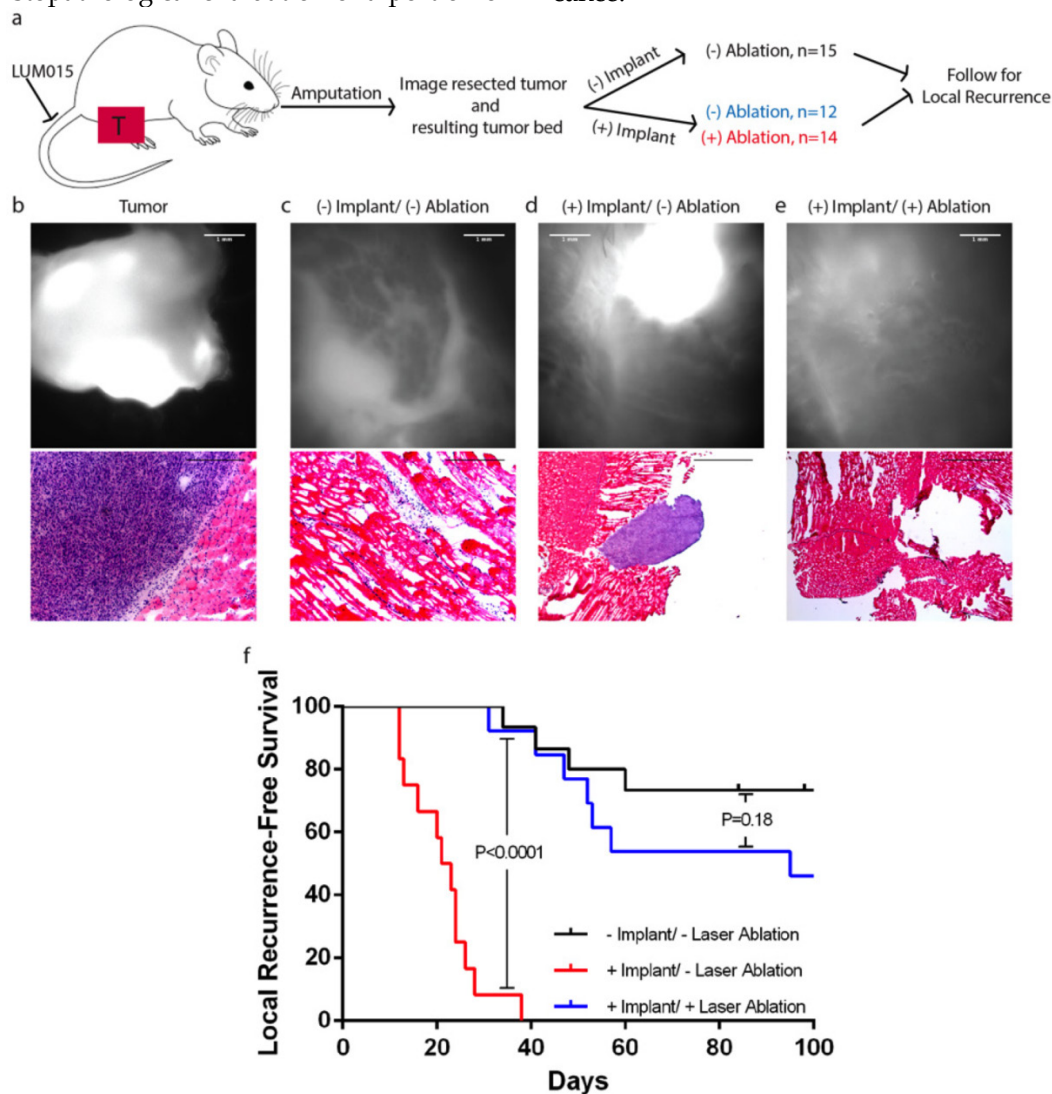
Figure 5. Intraoperative fluorescence-guided laser ablation has the potential to improve local recurrence outcomes. (a) An illustration of the experimental design. Mice with primary STS (T) received LUM015 six hours prior to amputation of the tumor-bearing limb. **(b)** The tumor was imaged to establish the fluorescence threshold and the tumor bed was then assessed for the presence of residual fluorescence. **(c)** Tissue was resected until no residual fluorescence was recorded. In one cohort of mice (-Implant/-Ablation, n=15), the surgical wound was immediately closed. **(d)** Otherwise, a piece of the resected tumor was re-implanted in the tumor bed. A group of 12 mice received no further treatment (+Impant/-Ablation). **(e)** Fluorescence-guided laser ablation was used to target and ablate the implanted residual disease in a third cohort of mice (+Implant/ +Ablation, n=14). **(f)** Survival plot showing that fluorescence-guided laser ablation of the implanted tumor significantly improves local recurrence-free survival, compared to mice who received an implant but no laser treatment (P<0.0001, Log-rank test). Scale bars= 500 μm unless otherwise noted.

In the + Implant/ - Laser Ablation cohort, all mice developed a measureable tumor within thirty days of surgery. In mice treated with laser ablation (n=14), there was a significant improvement in recurrence free survival (**P<0.0001, Figure 5F**) relative to mice left untreated (+ Implant/ - Laser Ablation). The difference in recurrence between mice treated with laser ablation (+ Implant/ + Laser Ablation) and mice with no residual fluorescence in the tumor bed and no simulated residual disease (- Implant/ - Laser Ablation) was not statistically significant (P=0.18). Additionally, laser ablation increased the time to measurable recurrence from a mean of 20.1 days to 61.2 days. Thus, fluorescence-guided laser ablation of simulated small-volume residual disease enhances recurrence free survival when compared to mice with untreated residual disease.

Discussion

In this study, we describe a novel integrated fluorescence detection and laser ablation system that is capable of removing sarcoma cells that have been labeled by a fluorescent imaging agent *in vivo*. Guided by the tumor detection system, the laser can precisely ablate fluorescent tissue with minimal disruption of adjacent normal tissue. This system is effective in reducing rates of local recurrence in a genetically engineered mouse model of soft tissue sarcoma (STS) with simulated small-volume residual disease. The imaging system identified areas of Cy5 (dye used in LUM015) fluorescence that correlated with cancer on histopathology as well as direct fluorescence imaging for YFP-expressing sarcoma cells. Moreover, tumor fluorescence from LUM015 detected by the imaging system was an effective driver of the galvo-mirrors controlling the laser such that simulated residual cancer was correctly identified and targeted for ablation.

We have previously developed the imaging system to identify residual cancer in the resection bed and have successfully utilized this system across species [3, 4]. Furthermore, LUM015 has been tested in humans in a Phase 1 clinical study showing that it is safe and that it preferentially labels tumor [5]. While imaging residual disease in the tumor bed is an important step toward eliminating microscopic cancer at the time of resection, there are instances when the precision limits of the human hand necessitate that a surgeon must either sacrifice a critical neurovascular structure or risk leaving behind tumor cells. An ablation system with sub-millimeter beam guidance and the ability to detect fluorescence from tumor tissue that is up to 8 mm below the imaged surface offers a means to remove residual cancer cells at the time of resection. Using this system, we were able to improve

recurrence free survival in mice with a simulation of small-volume residual disease. Previous clinical studies have demonstrated the capacity for fluorescence-guided surgery to improve rates of local recurrence. For example, the use of fluorescence guided surgery with 5-ALA was compared to white light surgery for malignant glioma resection, demonstrating a 1.5 month improvement in median survival [27], and for bladder tumor resection, resulting in a 37% decrease in the rate of local recurrence at 8 years [28]. We found that, using LUM015 fluorescence-guided laser ablation, our combined system achieved over a 50% improvement in local recurrence free survival. These results suggest that fluorescence-guided laser ablation may be a promising tool for ablating microscopic residual disease, especially in cases where there is a premium on preserving critical adjacent tissue.

In the course of this study, we identified no obvious adverse effects from the administration of the laser in the tumor bed. One possible limitation of this technology is the increased operative time needed for the tumor bed to be scanned and residual tumor to be ablated during surgery; however, if this technology can improve recurrence free survival similar to our proof-of-principle experiment, then we believe this would outweigh the risks associated with increased operative time. It is difficult to use the mouse experiments to estimate the increased operative time required to image and treat the much larger tumor beds encountered in humans. However, in the future we plan to test the integrated detection and laser ablation system in a clinical trial in dogs with naturally occurring sarcomas where the size of the tumor bed will more closely approximate what is encountered in human sarcoma patients.

The use of a protease-activated, fluorescence-guided intraoperative laser ablation system is novel and offers several potential advantages over previously described technologies. LUM015 is the first protease-activatable imaging agent for cancer detection to be tested for safety in humans (NCT01626066). This probe requires cleavage by proteases to release a quencher, allowing for fluorescence from the dye component of the probe to be detected. This cleavage-based functionality may then improve the sensitivity and specificity for labeling cancer [29]. Laser ablation is well described in surgery; however, here, we targeted laser ablation via molecular imaging of the LUM015 fluorescence signal rather than by direct visual guidance. In neurosurgery, advances have been made towards implementing a fluorescence-based intraoperative laser ablation system [30, 31]. However, that system has demonstrated neither the ability to remove microscopic residual disease, nor the poten-

tial to improve outcomes. Here we have demonstrated the ability to detect simulated small volume residual disease and ablate it with high precision while improving outcomes in a murine model.

While we used a sarcoma mouse model to test this system, this technology may be generalizable to other cancer models. Proteases that activate LUM015 are upregulated in a number of different cancers [32], suggesting that this approach to target cancers may be useful for other tumor types and anatomic sites. For example, this imaging and ablation system could be useful for omental caking in ovarian carcinoma and primary brain tumors. In both of these diseases, the size of local residual disease correlates with overall patient survival [33, 34], and in both of these cancers, proteases that can activate LUM015, such as cathepsin proteases, are overexpressed in tumor tissue [35, 36]. In ovarian cancer, an important aspect of management is optimal cytoreduction of omental metastasis, which indicates removal of all tumor nodules >1 cm. However, suboptimal debulking is a common problem, and, even with optimal debulking, difficult to resect disease may still be left behind. Similarly, the limits of the hand and human eye may necessitate that tumor tissue is left behind in the resection of primary brain tumors. Hence, in both of these clinical scenarios, there is a need to identify and ablate difficult to resect residual tumor burden.

There are, however, some locations in which cathepsin proteases may not serve as a suitable target for LUM015. For instance, the liver is known to express high levels of cathepsin proteases at baseline [37], rendering the protease-based nature of this probe impractical for this location. Nonetheless, one of the strengths of this technology lies in that laser ablation is guided by our sub-millimeter fluorescence detection system. A different enzymatic target could be chosen such that an activity based probe (ABP) could be used to identify, and treat, metastatic disease to the liver. Alternatively, ABPs could be structurally modified such that there is an improvement in localization to tumor and contrast between tumor and normal tissues [29, 38]. In theory, this system could be tailored to target any fluorescence-based ABP adapted to a suitable enzymatic target.

Despite the clinical implications of this study, there are some limitations. This was a proof-of-principle study using a prototype device; as such, there is still work to be done to generate a clinically feasible laser ablation module. Our current prototype is housed within a photoprotective box for safety reasons, making manipulation of the surgical stage and treatment area difficult. Additionally, to evaluate *in vivo* detection and ablation, we used an artificially generated simulation of residual disease to provide a more uniform amount of residual sarcoma between tumor beds. Despite the artificial nature of this experimental design, we found that every tumor bed implanted with a small volume of tumor, but not treated with laser ablation, developed a rapid tumor growth. Therefore, the transplanted tumor was able to incorporate successfully and we regard the lack of growth in those animals treated with the laser to represent successful ablation.

In the future, we plan to further develop the laser ablation prototype into a handheld system, which will integrate all current elements of the system to generate a device that would be suitable for use in the operating room. This could be tested in canine patients with naturally occurring spontaneous sarcomas to better model the scope of the imaging and ablation for a human patient. In future studies, we also plan to utilize mouse models of primary nerve sheath tumors [39] to further evaluate the use of laser ablation on tumors in and adjacent to critical structures.

Acknowledgements

Competing Interests

DGK is a member of the scientific advisory board and owns stock in Lumicell, Inc. DBS and JMF are employees of Lumicell, Inc. NR has founded a company called Zenalux Biomedical and she and other team members have developed technologies related to this work where the investigators or Duke may benefit financially if this system is sold commercially. The other authors declare that they have no conflicts of interest.

References

1. Cendan JC, Coco D, Copeland EM, 3rd. Accuracy of intraoperative frozen-section analysis of breast cancer lumpectomy-bed margins. Journal of the American College of Surgeons. 2005; 201: 194-8.
2. Pisters PW, Harrison LB, Leung DH, Woodruff JM, Casper ES, Brennan MF. Long-term results of a prospective randomized trial of adjuvant brachytherapy in soft tissue sarcoma. Journal of clinical oncology : official journal of the American Society of Clinical Oncology. 1996; 14: 859-68.
3. Mito JK, Ferrer JM, Brigman BE, Lee CL, Dodd RD, Eward WC, et al. Intraoperative detection and removal of microscopic residual sarcoma using wide-field imaging. Cancer. 2012; 118: 5320-30.
4. Eward WC, Mito JK, Eward CA, Carter JE, Ferrer JM, Kirsch DG, et al. A novel imaging system permits real-time in vivo tumor bed assessment after resection

of naturally occurring sarcomas in dogs. Clin Orthop Relat Res. 2013; 471: 834-42.

5. Whitley MJ, Cardona DM, Lazarides AL, Spasojevic I, Ferrer JM, Cahill J, Lee CL, Snuderl M, Blazer III DG, Hwang SE, Greenup RA, Mosca PJ, Mito JK, Cuneo KC, Larrier NA, O'Reilly EK, Riedel RF, Eward WC, Strasfeld DB, Fukumara D, Jain RK, Lee WD, Griffith LG, Bawendi MG, Kirsch DG, and Brigman BE. A Mouse-human Phase I co-clinical trial of a protease-activated fluorescent probe for imaging cancer. Science Translational Medicine. In Press.

6. Pleijhuis RG, Crane L, van Oosten M, van Dam G, Ntziachristos V. Optical Imaging Applications in Cancer Research and Treatment. Cancer – Cares, Treatments and Preventions. USA: iConcept Press; 2014.

7. Bouvet M, Hoffman RM. Glowing tumors make for better detection and resection. Science translational medicine. 2011; 3: 110fs10.

8. Hoffman RM, Bouvet M. Shedding (killer) light on tumors. Semin Thorac Cardiovasc Surg. 2012; 24: 235-7.

9. Hiroshima Y, Maawy A, Zhang Y, Sato S, Murakami T, Yamamoto M, et al. Fluorescence-guided surgery in combination with UVC irradiation cures metastatic human pancreatic cancer in orthotopic mouse models. PloS one. 2014; 9: e99977.

10. Yano S, Miwa S, Kishimoto H, Uehara F, Tazawa H, Toneri M, et al. Targeting tumors with a killer-reporter adenovirus for curative fluorescence-guided surgery of soft-tissue sarcoma. Oncotarget. 2015; 6: 13133-48.

11. Boppart SA, Herrmann J, Pitris C, Stamper DL, Brezinski ME, Fujimoto JG. High-resolution optical coherence tomography-guided laser ablation of surgical tissue. The Journal of surgical research. 1999; 82: 275-84.

12. Saksena S, Hussain SM, Gielchinsky I, Gadhoke A, Pantopoulos D. Intraoperative mapping-guided argon laser ablation of malignant ventricular tachycardia. The American journal of cardiology. 1987; 59: 78-83.

13. Mito JK, Min HD, Ma Y, Carter JE, Brigman BE, Dodd L, et al. Oncogene-dependent control of miRNA biogenesis and metastatic progression in a model of undifferentiated pleomorphic sarcoma. J Pathol. 2013; 229: 132-40.

14. Jonkers J, Meuwissen R, van der Gulden H, Peterse H, van der Valk M, Berns A. Synergistic tumor suppressor activity of BRCA2 and p53 in a conditional mouse model for breast cancer. Nature genetics. 2001; 29: 418-25.

15. Dankort D, Filenova E, Collado M, Serrano M, Jones K, McMahon M. A new mouse model to explore the initiation, progression, and therapy of BRAFV600E-induced lung tumors. Genes & development. 2007; 21: 379-84.

16. Jackson EL, Willis N, Mercer K, Bronson RT, Crowley D, Montoya R, et al. Analysis of lung tumor initiation and progression using conditional expression of oncogenic K-ras. Gene Dev. 2001; 15: 3243-8.

17. Kirsch DG, Dinulescu DM, Miller JB, Grimm J, Santiago PM, Young NP, et al. A spatially and temporally restricted mouse model of soft tissue sarcoma. Nature medicine. 2007; 13: 992-7.

18. Suhm N, Gotz MH, Fischer JP, Loesel F, Schlegel W, Sturm V, et al. Ablation of neural tissue by short-pulsed lasers--a technical report. Acta neurochirurgica. 1996; 138: 346-9.

19. Hu X, Fang Q, Cariveau MJ, Pan X, Kalmus GW. Mechanism study of porcine skin ablation by nanosecond laser pulses at 1064, 532, 266, and 213 nm. IEEE Journal of Quantum Electronics. 2001; 37: 322.

20. Ogura M, Sato S, Ishihara M, Kawauchi S, Arai T, Matsui T, et al. Myocardium tissue ablation with high-peak-power nanosecond 1,064- and 532-nm pulsed lasers: influence of laser-induced plasma. Lasers in surgery and medicine. 2002; 31: 136-41.

21. Vogel A, Venugopalan V. Mechanisms of pulsed laser ablation of biological tissues. Chemical reviews. 2003; 103: 577-644.

22. Fu HL, Mueller JL, Javid MP, Mito JK, Kirsch DG, Ramanujam N, et al. Optimization of a widefield structured illumination microscope for non-destructive assessment and quantification of nuclear features in tumor margins of a primary mouse model of sarcoma. PloS one. 2013; 8: e68868.

23. Parthasarathy AB, Tom WJ, Gopal A, Zhang X, Dunn AK. Robust flow measurement with multi-exposure speckle imaging. Optics express. 2008; 16: 1975-89.

24. Bydlon TM, Kennedy SA, Richards LM, Brown JQ, Yu B, Junker MK, et al. Performance metrics of an optical spectral imaging system for intra-operative assessment of breast tumor margins. Opt Express. 2010; 18: 8058-76.

25. Brown JQ, Bydlon TM, Richards LM, Yu B, Kennedy SA, Geradts J, et al. Optical assessment of tumor resection margins in the breast. IEEE J Sel Top Quantum Electron. 2010; 16: 530-44.

26. Harlaar NJ, Hesselink JW, de Jong JS, van Dam GM. Bioluminescence as Gold Standard for Validation of Optical Imaging Modalities in Peritoneal Carcinomatosis Animal Models. Eur Surg Res. 2010; 45: 308-13.

27. Stummer W, Pichlmeier U, Meinel T, Wiestler OD, Zanella F, Reulen HJ, et al. Fluorescence-guided surgery with 5-aminolevulinic acid for resection of malignant glioma: a randomised controlled multicentre phase III trial. The Lancet Oncology. 2006; 7: 392-401.

28. Denzinger S, Burger M, Walter B, Knuechel R, Roessler W, Wieland WF, et al. Clinically relevant reduction in risk of recurrence of superficial bladder cancer using 5-aminolevulinic acid-induced fluorescence diagnosis: 8-year results of prospective randomized study. Urology. 2007; 69: 675-9.

29. Blum G, von Degenfeld G, Merchant MJ, Blau HM, Bogyo M. Noninvasive optical imaging of cysteine protease activity using fluorescently quenched activity-based probes. Nat Chem Biol. 2007; 3: 668-77.

30. Noguchi M, Aoki E, Yoshida D, Kobayashi E, Omori S, Muragaki Y, et al. A novel robotic laser ablation system for precision neurosurgery with intraoperative 5-ALA-induced PpIX fluorescence detection. Medical image computing and computer-assisted intervention : MICCAI International Conference on Medical Image Computing and Computer-Assisted Intervention. 2006; 9: 543-50.

31. Liao H, Noguchi M, Maruyama T, Muragaki Y, Kobayashi E, Iseki H, et al. An integrated diagnosis and therapeutic system using intra-operative 5-aminolevulinic-acid-induced fluorescence guided robotic laser ablation for precision neurosurgery. Medical image analysis. 2012; 16: 754-66.

32. Koblinski JE, Ahram M, Sloane BF. Unraveling the role of proteases in cancer. Clinica chimica acta; international journal of clinical chemistry. 2000; 291: 113-35.

33. Polterauer S, Vergote I, Concin N, Braicu I, Chekerov R, Mahner S, et al. Prognostic value of residual tumor size in patients with epithelial ovarian cancer FIGO stages IIA-IV: analysis of the OVCAD data. Int J Gynecol Cancer. 2012; 22: 380-5.

34. Yoo H, Kim YZ, Nam BH, Shin SH, Yang HS, Lee JS, et al. Reduced local recurrence of a single brain metastasis through microscopic total resection. J Neurosurg. 2009; 110: 730-6.

35. Nishikawa H, Ozaki Y, Nakanishi T, Blomgren K, Tada T, Arakawa A, et al. The role of cathepsin B and cystatin C in the mechanisms of invasion by ovarian cancer. Gynecologic oncology. 2004; 92: 881-6.

36. Levicar N, Nuttall RK, Lah TT. Proteases in brain tumour progression. Acta neurochirurgica. 2003; 145: 825-38.

37. Moles A, Tarrats N, Fernandez-Checa JC, Mari M. Cathepsins B and D drive hepatic stellate cell proliferation and promote their fibrogenic potential. Hepatology. 2009; 49: 1297-307.

38. Edgington LE, Berger AB, Blum G, Albrow VE, Paulick MG, Lineberry N, et al. Noninvasive optical imaging of apoptosis by caspase-targeted activity-based probes. Nature medicine. 2009; 15: 967-73.

39. Dodd RD, Mito JK, Eward WC, Chitalia R, Sachdeva M, Ma Y, et al. NF1 Deletion Generates Multiple Subtypes of Soft-Tissue Sarcoma That Respond to MEK Inhibition. Molecular Cancer Therapeutics. 2013; 12: 1906-17.